

Life-cycle-cost optimization for the wind load design of tall buildings equipped with TMDs

Ilaria Venanzi^{*1}, Laura Ierimonti^{1a} and Luca Caracoglia^{2b}

¹Department of Civil and Environmental Engineering, University of Perugia, Via G. Duranti 93, Perugia, Italy

²Department of Civil and Environmental Engineering, Northeastern University, 400 Snell Engineering Center, 360 Huntington Ave., MA 02115, USA

(Received June 24, 2018, Revised November 22, 2019, Accepted February 4, 2020)

Abstract. The paper presents a Life-Cycle Cost-based optimization framework for wind-excited tall buildings equipped with Tuned Mass Dampers (TMDs). The objective is to minimize the Life-Cycle Cost that comprises initial costs of the structure, the control system and costs related to repair, maintenance and downtime over the building's lifetime. The integrated optimization of structural sections and mass ratio of the TMDs is carried out, leading to a set of Pareto optimal solutions. The main advantage of the proposed methodology is that, differently from the traditional optimal design approach, it allows to perform the unified design of both the structure and the control system in a Life Cycle Cost Analysis framework. The procedure quantifies wind-induced losses, related to structural and nonstructural damage, considering the stochastic nature of the loads (wind velocity and direction), the specificity of the structural modeling (e.g., non-shear-type vibration modes and torsional effects) and the presence of the TMDs. Both serviceability and ultimate limit states related to the structure and the TMDs' damage are adopted for the computation of repair costs. The application to a case study tall building allows to demonstrate the efficiency of the procedure for the integrated design of the structure and the control system.

Keywords: tall buildings; wind loads; non-prescriptive design; wind tunnel tests; tuned mass dampers; cost-based optimization

1. Introduction

Wind-induced vibrations of high-rise buildings are often reduced by means of control systems (Qiusheng *et al.* 1999, Kareem *et al.* 1999, Palmeri *et al.* 2004, Ross *et al.* 2015, Aly 2015), especially Tuned Mass Dampers (TMDs). The main advantage of the TMD installation is the reduction of the vibration level experienced by the building (Ricciardelli 1999, Said and Matsagar 2018), with a consequent reduction of damage-related losses and occupants' discomfort (Kwok *et al.* 2015). On the other hand, the installation of TMDs requires a significant investment for the stakeholders, related to the initial cost of the device, its maintenance and the loss of income due to the floor's surface necessary for the installation. Another problem in the design of TMDs for tall buildings is that the presence of uncertainties related to the structure and the wind load may lead to possible mistuning of the device.

In this perspective, Life-Cycle Cost Analysis (LCCA) can be a powerful tool for the integrated design of the building and its control system. LCCA is an approach

adopted for the cost-based structural design capable of computing the total lifetime cost accounting for initial expense, repair and maintenance cost, downtime cost and disposal cost, relating expenditures to the probability of exceeding specific limit states. The approach can account for all the possible sources of uncertainties related to the design of the controlled tall building (Cui and Caracoglia 2018, Venanzi *et al.* 2018). LCCA is based on Performance-Based Design (PBD), a methodology aimed at ensuring pre-defined structural performance levels, recently extended to wind-excited structures (Bashor and Kareem 2007, Ciampoli and Petrini 2012, Pozzuoli *et al.* 2013, Bernardini *et al.* 2013, Chuang and Spence 2017, Ierimonti *et al.* 2017, 2018, 2019).

When dealing with the optimal design of wind-exposed tall buildings equipped with TMDs, it is advisable to account for the trade-off between the cost of the control devices, the loss of income due to the installation space and the cost of the structural stiffening. The achievement of significant vibration mitigation can be obtained by increasing the mass ratio of the TMD or by stiffening the structure. If the TMD cost increases, the structural cost decreases, as it is necessary to reduce the strength of the main lateral wind-load resisting system. Following this consideration, the optimal solution can be obtained from the integrated optimization of TMDs and structure, as a compromise between the initial cost components. Conversely, the initial cost increase provides reduction of repair cost or indirect costs related to discomfort. Although the simultaneous optimization of the structure and the

*Corresponding author, Professor

E-mail: ilaria.venanzi@unipg.it

^aPh. D.

E-mail: laura.ierimonti@unipg.it

^bAssociate Professor

E-mail: lucac@coe.neu.edu

control system is evidently advisable, just a few literature papers deal with integrated design of both the structure and the TMD (Huang *et al.* 2011).

The main aim of the paper is to propose a methodology for the integrated optimal design of structure and TMDs for tall buildings exposed to wind load. The proposed methodology is based on a systematic LCCA framework, designated as Life-Cycle Cost Wind Design (LCCWD), that is specific for tall buildings and has been recently introduced by the Authors (Ierimonti *et al.* 2017, 2018, 2019). The procedure quantifies wind-induced direct and indirect losses, related to damage of nonstructural elements and discomfort, by considering the stochastic nature of wind velocity and direction, nonlinear vibration modes, the combination of the flexural and torsional response and the presence of TMDs. In this paper the procedure is extended to account for structural damage related to the achievement of ultimate limit states (for axial force, bending and shear) and to account for damage related to the achievement of the maximum allowable TMDs' stroke. An application to a case study is carried out to demonstrate the effectiveness of the procedure and to investigate the influence on the results of lifetime duration and the effect of different weights assigned to the terms of the objective function.

2. The LCCWD of tall buildings equipped with TMDs: improved formulation accounting for damage related to both serviceability and ultimate limit states

2.1 Initial requirements of the procedure

The procedure requires the definition of information:

- 1) A *structural model* of the tall building (characterized by structural parameters, *SP*) equipped with a control system (*CS*) consisting in a set of TMDs. It is assumed that the response is dominated by the three fundamental lateral vibration modes (two lateral bending modes and one torsional mode) without inter-modal coupling. The power-law function depending on coordinate z (floor height) is employed to describe the mode shapes. The presence of TMDs on top is taken into account using the Warburton's formulation of stiffness and damping.
- 2) A *wind hazard model*, characterized by exploiting wind tunnel data obtained with conventional High Frequency Force Balance (HFFB) tests (Chen *et al.* 2014, Xie and Garber 2014) or, indirectly, by integrating synchronous wind pressure measurements. The mean annual wind speed (V_{ref}) and direction (θ) are the components of the intensity measure (*IM*) vector. Their joint probability density function $f(V_{ref}, \theta)$ is used to account for the variability of the wind load intensity.
- 3) A *fragility model*, i.e., fragility curves (or surfaces), representing the probability of damage occurrence, given a specific value of the selected Engineering Demand Parameter (EDP). The choice of the EDPs depends on the selected damage states. Most serviceability damage states for tall buildings are acceleration-dependent or drift-dependent.

- 4) A *cost model*, characterized by the initial cost of the structure and the control system, the maintenance cost, the unit costs associated with the replacement or repair of the elements and the indirect losses, like those related to business downtime.

2.2 Background on the LCCWD methodology

By exploiting the items mentioned in Section 2.1, the following steps are carried out in order to compute the expected life-cycle cost.

2.2.1 Structural analysis

Consider a cantilever vertical structure and consider a local Cartesian reference system whose z axis is coincident with the center of mass of all structural cross-sections (floors). The equations of motion at time t are expressed as

$$\mathbf{M}(z)d''(z, t) + \mathbf{C}(z)d'(z, t) + \mathbf{K}(z)d(z, t) = \mathbf{F}(z, t) \quad (1)$$

where \mathbf{M} , \mathbf{C} and \mathbf{K} are the matrix operators of mass, structural damping and structural stiffness per unit length of the structure, $\mathbf{F}(z, t)$ is the vector of the wind load. The structural analysis is carried out in the frequency domain and the motion of the structure is expressed as a series of classical normal modes

$$d(z, t) = \sum_k \Phi_k(z)p_k(t) \quad (2)$$

where Φ_k is the k -th eigenvector and p_k is the vector of the k -th principal coordinate. The generalized forces and moments associated with the experimentally measured turbulent wind pressures on the building's surface (Tse *et al.* 2014, Xu and Xie 2015) can be written as

$$F_{Q_{ik}}(t) = \int_0^H f_{ik}(z, t) \Phi_k(z) dz \quad (3a)$$

$$F_{Q_{i\psi}}(t) = \int_0^H f_{i\psi}(z, t) \Phi_\psi(z) dz \quad (3b)$$

In the previous equations $k=\{x, y\}$ is the index denoting the two principal response components (the displacements of the floor geometric centers in directions x and y) and ψ indicates the torsional rotation about the vertical axis z , $f_{ik}(z, t)$ is the i -th realization of the experimental aerodynamic force per unit height in the k direction calculated at height z (for example by local pressure integration), $f_{i\psi}(z, t)$ is the i -th realization of the aerodynamic floor torque, H is the total height of the building; $\Phi_k(z) = (z/H)^{\gamma_k}$ and $\Phi_\psi(z) = (z/H)^{\gamma_\psi}$ are the fundamental mode shapes with $\gamma_k, \gamma_\psi > 0$ power-law exponents. The response power spectral densities of the building and the TMD are consequently obtained after manipulation of the previous equations as

$$S_{Q_{ik}}(n) = |H_k(n)|^2 S_{F_{Q_{ik}}}(n) \quad (4a)$$

$$S_{Q_{i\psi}}(n) = \varepsilon_\psi |H_\psi(n)|^2 S_{F_{Q_{i\psi}}}(n) \quad (4b)$$

$$S_{Q_{TMD_{ik}}}(n) = |H_{TMD,k}(n)|^2 S_{F_{Q_{ik}}}(n) \quad (4c)$$

where n is the frequency (Hz); $S_{F_{Qik}}$ is the one-sided power spectral density of the generalized load of the k -th mode with i -th realization; $S_{F_{Qi\psi}}$ is the one-sided power spectral density of the generalized torque with i -th realization; ε_k is a correction factor used to adjust the experimental evaluation of the uniformly distributed base torque along the height which can be calculated as a function of the power-law exponent of the γ_ψ (Holmes *et al.* 2003, Tallin and Ellingwood 1985). The formulation implies that there is one TMD acting in each of the principal planes of deformation (along x and y directions).

$|H_k(n)|$, $|H_\psi(n)|$ and $|H_{TMD,k}(n)|$ are the absolute values of the modal transfer functions of the structure and the TMD (Xu *et al.* 1992)

$$|H_k(n)|^2 = \frac{(\chi^2 - \lambda^2)^2 + 4\lambda^2\chi^2\zeta_{02}^2}{(2\pi n_{0k}^4)M_k^2(a^2 + b^2)} \quad (5a)$$

$$|H_\psi(n)|^2 = \frac{1}{(2\pi n_{0\psi}^4)M_\psi^2 \left[\left(1 - \left(\frac{n_\psi}{n_{0\psi}}\right)^2\right)^2 + 4\xi_{0\psi}^2 \left(\frac{n_\psi}{n_{0\psi}}\right)^2 \right]} \quad (5b)$$

$$|H_{TMD,k}(n)|^2 = \frac{\lambda^2}{a^2 + b^2} \quad (5c)$$

where $a = \lambda^4 - \lambda^2(1 + \chi^2 + \mu\chi^2 + 4\zeta_{0,k}\zeta_k\chi) + \chi^2$; $b = 2\lambda[\zeta_k\chi(1 - \lambda^2 - \mu\lambda^2) + \zeta_{0,k}(\chi^2 - \lambda^2)]$; m_k and $n_k = 1/2\pi\sqrt{k_k/m_k}$ are the mass and the frequency of the TMD; $\xi_k = c_k/(2\sqrt{k_k m_k})$ is the reference modal damping ratio; $\mu = m_k/M_k$ is the TMD mass ratio in the two principal directions, $\chi = n_k/n_{0k}$ and $\lambda = n/n_{0k}$ are the frequency ratios; M_k is the building modal mass in the two principal directions; M_ψ is the building modal, mass moment of inertia.

The standard deviations of the structural response components (σ_{ik} and $\sigma_{i\psi}$) and the standard deviations of the TMD displacements ($\sigma_{TMD,ik}$) are computed for the i -th wind tunnel load realization with the following equations,

$$\sigma_{ik}^2 = \int_0^{+\infty} S_{Q_{ik}}(n)dn \quad (6a)$$

$$\sigma_{i\psi}^2 = \int_0^{+\infty} S_{Q_{i\psi}}(n)dn \quad (6b)$$

$$\sigma_{TMD,ik}^2 = \int_0^{+\infty} S_{Q_{TMD,ik}}(n)dn \quad (6c)$$

The peak lateral displacements and the peak acceleration at the top floor ($z = H$) are computed, for the i -th wind tunnel realization of the load, by combining flexural and torsional response projected in the two main directions x and y . The peak response components are assumed as simultaneous, as it is commonly done in frequency domain response computation.

$$D_{ik}(z) = \frac{[\bar{D}_{ik}\Phi_k(z) \pm \bar{D}_{i\psi k}\Phi_\psi(z)]}{\sqrt{[g_{ik}\sigma_{ik}\Phi_x(z)]^2 + [g_{i\psi}\sigma_{i\psi k}\Phi_\psi(z)]^2}} \quad (7a)$$

for $k = x, y$

$$a_i(z) = \frac{1}{\sqrt{[g_{ix}^a\sigma_{ix}^a\Phi_x(z)]^2 + [g_{iy}^a\sigma_{iy}^a\Phi_y(z)]^2 + [g_{i\psi x}^a\sigma_{i\psi x}^a\Phi_\psi(z)]^2 + [g_{i\psi y}^a\sigma_{i\psi y}^a\Phi_\psi(z)]^2}} \quad (7b)$$

where \bar{D}_{ik} ($k=x, y$) are the mean horizontal responses in the x and y horizontal-plane directions; $\bar{D}_{i\psi k}$ ($k=x, y$) are the torsional components of the response in the lateral, horizontal directions; g_{ik} are the peak factors computed in accordance with the structural response spectrum and Davenport's theory (Davenport 1964, 1967), σ_{ik} and σ_{ix}^a are the standard deviations of D and a , $\sigma_{i\psi k}$ and $\sigma_{i\psi k}^a$ are the torsional-dependent standard deviations of the response; the x and y lateral displacement or acceleration components, related to the mean torsional response, are characterized by the subscript ψ .

The peak TMDs displacements can be computed, according to Davenport's formulation (Davenport 1967), as

$$D_{TMD,ik} = g_{ik}\sigma_{TMD,ik} \quad (8)$$

2.2.2 Fragility analysis

The annual damage probability can be computed through the PEER (Pacific Earthquake Engineering Research) convolution integral equation (Cornell and Krawinkler 2000, PEER-TBI 2010, Kunnath 2006) as follows

$$P_j^a(z) = \int \int \int P(DS_j(z)|EDP(V_{ref}, \theta, CS))f(EDP|V_{ref}, \theta, CS) \quad (9)$$

$$f(V_{ref}, \theta)dEDPdV_{ref}d\theta$$

In the previous equation DS_j is the j -th damage state; EDP is the vector collecting the engineering demand parameters (i.e., the structural response components) inducing the damage; $P(DS_j|EDP)$ is the structural fragility curve (i.e., the complementary cumulative distribution function of DS_j , conditional on the occurrence of EDP); $f(EDP|V_{ref}, \theta, CS)$ is the probability density function (PDF) of EDP conditional on V_{ref} , θ and CS ; $f(V_{ref}, \theta)$ is the joint PDF of V_{ref} and θ .

The t -year probability of exceeding the damage state j is defined as

$$P_j^t(z) = 1 - [1 - P_j^a(z)] \quad (10)$$

The probability of exceeding the j -th damage state given the mean arrival rate of the wind hazard (ν) per unit time is defined as follows

$$P_j(z) = -\frac{1}{\nu t} \log_e [1 - P_j^t(z)] \quad (11)$$

with ν being the annual occurrence rate of the wind

storms.

2.2.3 Cost analysis including maintenance, repair and indirect losses

The total expected life-cycle cost is computed as follows (Wen and Kang 2001)

$$E[C(t)] = C_0 + \frac{1}{\lambda} \left\{ C_m(t) + E \left[\sum_z C_r(t, z) \right] + E \left[\sum_z C_{IL}(t, z) \right] \right\} (1 - e^{-\lambda t}) \quad (12)$$

where the operator $E[\cdot]$ denotes expected value, C_0 is the initial cost of the structure-TMDs system, $C_m(t)$ is the maintenance cost assumed as a deterministic quantity function of the lifetime duration t , $E[\sum_z C_r(t, z)]$ is the expected value of the summation over the floors of the repair/intervention costs during lifetime t , $E[\sum_z C_{IL}(t, z)]$ is the expected value of the summation over the floors of indirect losses (IL) and λ is the discount rate per year.

The initial cost of the structure-TMDs system (C_0) can be assumed, as a first approximation, as a deterministic quantity. It is the sum of two components

$$C_0 = C_{0s} + C_{0cs} \quad (13)$$

where C_{0s} is the initial cost of the building (structural members, floors, nonstructural components) and C_{0cs} is the cost of the control system, i.e., the cost of the set of TMDs.

The maintenance cost (C_m) includes ordinary repair and substitution of structural and non-structural components and it is defined as the sum of a percentage α_m of C_{0s} and a percentage β_m of C_{0cs}

$$C_m = \alpha_m \cdot C_{0s} + \beta_m \cdot C_{0cs} \quad (14)$$

The repair cost is computed as follows

$$E[C_r(t, z)] = E \left[\sum_{l=1}^L \sum_{j=1}^K v \hat{C}_j^r P_j^r(z) \right] \quad (15)$$

In the previous expression z is the floor's height; l is the loading occurrence number; L is the total number of loading occurrences between time 0 and time t (in years) assumed as a Poisson counting process for extreme events; j is the damage state number; K is the total number of damage states; \hat{C}_j^r is the total repair cost for the j^{th} damage state (deterministic), v is the mean occurrence rate of the hazard, P_j^r is the probability of exceeding the j^{th} damage state given the occurrence of a wind event. By exploiting Eq. (11) and considering the number of unit elements n_j at the floor at height z , the repair cost becomes

$$E[C_r(t, z)] = E \left[\sum_{l=1}^L \sum_{j=1}^K n_j(z) C_j^r \left[-\frac{1}{vt} \log_e (1 - P_{t,j}^r(z)) \right] \right] \quad (16)$$

where C_j^r is the repair costs referred to unit elements. In the previous expression the costs are cumulated by accounting for mutually excluding limit state damages, i.e., a major damage level and cost, associated with an EDP, must

exclude the corresponding minor damage. The downtime cost related to repair activities is not explicitly considered, but it could be included by increasing the repair costs associated with unit elements.

The indirect losses are computed as follows

$$E[C_{IL}(t, z)] = E \left[\sum_{l=1}^L v \hat{C}_{IL} P_j^{il}(z) \right] \quad (17)$$

where $E[C_{IL}(t, z)]$ is the expected value of the indirect losses, which comprise loss related to business downtime due to occupants' discomfort. The coefficient \hat{C}_{IL} is the unit cost associated with the business downtime; P_j^{il} is the probability of exceeding the acceleration level threshold, given by Eq. (11).

3. Integrated optimal design of tall buildings with Tuned Mass Dampers

The parameters to be optimized are stored in the design variables' vector that collects the mass ratio of the TMDs and the structural parameters

$$\mathbf{x} = (\mu, \alpha) \quad (18)$$

where $\mu = m_k/M_k$ is the mass ratio, i.e., the ratio between the mass of the TMD (m_k) and the first modal mass of the of the lateral, translating bending mode of the structure (M_k) that is assumed equal in both directions $k=\{x, y\}$, and α is a coefficient multiplying the thickness of the structural elements with respect to nominal design values, in order to vary the stiffness and the mass of the structure. It is assumed that the coefficient μ is independent of α , for small variation of the structural members.

The optimization problem can be stated as follows

$$\arg \min_{\mathbf{x}} Z(\mathbf{x}, t) = \{ \mathbf{x} \mid \mathbf{x}_{min} \leq \mathbf{x} \leq \mathbf{x}_{max} \} \quad (19)$$

where the design variables' vector is constrained by upper and lower limit values \mathbf{x}_{min} and \mathbf{x}_{max} , respectively. By combining Eqs. (12) to (17), the objective function Z can be defined as the weighed sum of the different components of the total expected life-cycle cost $E[C(\mathbf{x}, t)]$

$$Z(\mathbf{x}, t) = p_1 \left\{ C_0(\mathbf{x}) + [C_m(\mathbf{x}, t)] \frac{1}{\lambda} (1 - e^{-\lambda t}) \right\} + p_2 \left\{ E \left[\sum_z C_r(\mathbf{x}, t, z) \right] + E \left[\sum_z C_{IL}(\mathbf{x}, t, z) \right] \frac{1}{\lambda} (1 - e^{-\lambda t}) \right\} \quad (20)$$

where p_1 and p_2 are the weight coefficients. The choice of the weight coefficients is crucial for design, as it can target the optimization procedure towards different outcomes. Higher values of p_1 lead to a greater reduction of initial costs while higher values of p_2 provide greater reduction of lifetime losses. The genetic algorithm is selected for solving the optimization problem (Sivanandam and Deepa 2008).

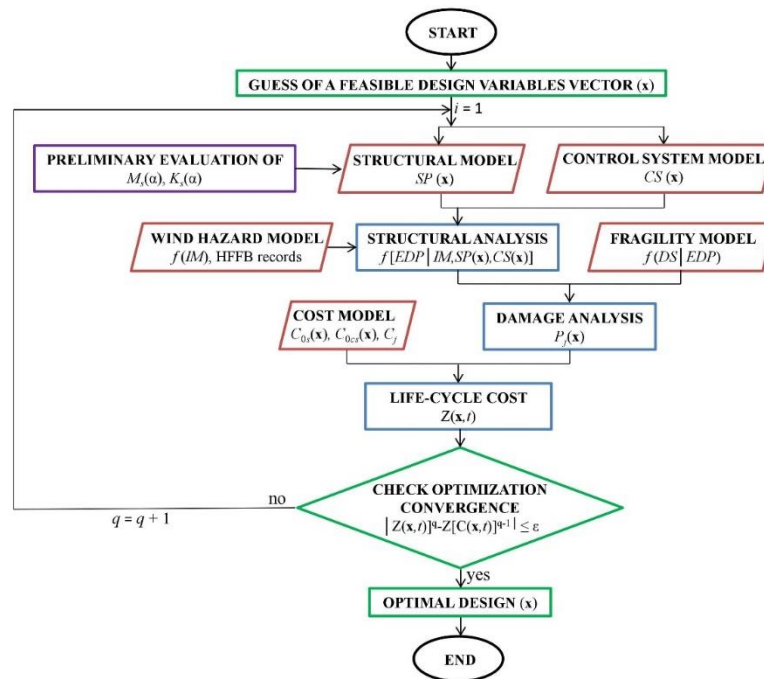


Fig. 1 Flow chart of the optimization procedure

Fig. 1 shows the flow chart of the optimization procedure. Before performing the optimization, an off-line preliminary evaluation of the structural mass and stiffness matrices $[M_s(\alpha), K_s(\alpha)]$ corresponding to several preset values of the coefficient α is performed. Subsequently, the genetic algorithm selects a guess value of the design variables' vector $\mathbf{x}=(\alpha, \mu)$ that falls within the feasible range, defined by \mathbf{x}_{\min} and \mathbf{x}_{\max} . The global mass and stiffness matrices of the building with TMDs characterizing the structural model $SP(\mathbf{x})$ are computed using vector \mathbf{x} and the closest set $[M_s(\alpha), K_s(\alpha)]$ among those previously evaluated. The structural analysis is carried out using a probabilistic wind hazard model, leading to the probability distribution of the EDPs conditional on the wind load (IM), the structural model (SP) and the control system (CS). By exploiting the fragility model, the damage analysis is carried out in order to compute the probability of exceeding the selected damage states P_j . The life-cycle cost $E[C(\mathbf{x},t)]$ is calculated based on the selected cost model. The optimization algorithm performs the check of the optimization convergence at each step q to iteratively find the solution. If the reduction of the expected LCC with respect to the previous iteration is smaller than a preset threshold ϵ , the q -th iteration value of the design variable vector is the optimal solution. Otherwise, new trial values of \mathbf{x} are analyzed until converge is reached.

4. Damage analysis including serviceability and ultimate limit states

In the previous LCCWD formulation (Ierimonti *et al.* 2017, 2018, 2019) it was assumed that damage in tall buildings is predominantly non-structural and occurs on secondary structural elements. Various cost-based solutions

were analyzed and compared. In the present paper, since the main objective is to perform an integrated optimal design considering the structure and the TMD system, the occurrence of structural damage associated to both serviceability and ultimate limit states conditions must be considered.

For this reason, the proposed enhanced LCCWD procedure allows accounting for several types of losses, as reported in Table 1 and explained in the following

Type 1 are direct losses related to drift-dependent damage to non-structural elements that occur to glass façades, partition walls, etc. The EDP is the peak inter-story drift ratio, defined as

$$IDR_{ik}(z, \mathbf{x}) = \frac{D_{ik}(z, \mathbf{x}) - D_{ik}(z - h_{int}, \mathbf{x})}{h_{int}} \quad (21)$$

Table 1 Losses considered within the LCCWD procedure

Item no.	Type of loss	Engineering Demand Parameters	Damaged elements	Limit state type
1	Direct/non-structural	Peak inter-story drift	Glass façades, partition walls	Serviceability
2	Direct/non-structural	Peak acceleration	Suspended ceilings, pipes	Serviceability
3	Direct/structural	Peak Demand-to-Capacity Index (DCI)	Columns, beams, bracings	Ultimate
4	Direct/structural	Peak stroke	TMD	Ultimate
5	Indirect/comfort related	Peak acceleration	-	Serviceability

where h_{int} is the inter-story height; D_{ik} can be computed through Eq. (7a) (i -th realization and $k=x, y$). For each type of non-structural element, one or more fragility curves associated with specific damage levels can be defined as a function of the IDR (e.g. in the case of glass façades: glass cracking, glass falling from frame; Ierimonti *et al.* 2017).

Type 2 are direct losses, related to acceleration-dependent damage to non-structural elements that occur for example to suspended ceilings. The EDP is the peak floor acceleration, computed with Eq. (7b).

Type 3 are direct losses related to failure of structural elements. Only columns are considered for strength verifications, as they are structural elements that predominantly influence the mass and stiffness matrices of the building. Other element types, like beams, girders and cross-bracings, can be included in the framework. Adopting the shear-type hypothesis, the peak bending moments of each column for the i -th wind load realization, can be computed as

$$M_{ki}(z, \mathbf{x}) = \chi_k(z, \mathbf{x}) IDR_{ik}(z, \mathbf{x}) \frac{h_{int}^2}{2} \quad (22)$$

where χ_k ($k=x, y$) are the flexural stiffnesses of the structural elements, and the product $IDR_{ik}h_{int}$ is the peak horizontal floor's displacement.

The peak shear forces are calculated (by equilibrium) as

$$V_{ki}(z, \mathbf{x}) = 2 \frac{M_{ki}(z, \mathbf{x})}{h_{int}} = \chi_k(z, \mathbf{x}) IDR_{ik}(z, \mathbf{x}) h_{int} \quad (23)$$

The demand-to-capacity indices (DCIs) are adopted as the parameters for fragility estimation (Simiu, 2011). DCIs, for strength verifications, must be smaller than unity. For steel beam/column verifications, subjected to combined bending moments and axial forces, DCIs are defined as

$$\begin{cases} DCI_{MNI}(z) = \frac{P_i(z, \mathbf{x})}{\varphi P_n(z, \mathbf{x})} + \frac{8}{9} \left(\frac{M_{xi}(z, \mathbf{x})}{\varphi M_{nx}(z, \mathbf{x})} + \frac{M_{yi}(z, \mathbf{x})}{\varphi M_{ny}(z, \mathbf{x})} \right) \leq 1 \\ \quad \text{when } \frac{P_i(z, \mathbf{x})}{\varphi P_n(z, \mathbf{x})} \geq 0.2 \\ DCI_{MNI}(z) = \frac{P_i(z, \mathbf{x})}{2\varphi P_n(z, \mathbf{x})} + \left(\frac{M_{xi}(z, \mathbf{x})}{\varphi M_{nx}(z, \mathbf{x})} + \frac{M_{yi}(z, \mathbf{x})}{\varphi M_{ny}(z, \mathbf{x})} \right) \leq 1 \\ \quad \text{when } \frac{P_i(z, \mathbf{x})}{\varphi P_n(z, \mathbf{x})} < 0.2 \end{cases} \quad (24)$$

For steel column verifications with respect to shear, DCIs are defined as

$$DCI_{Vki}(z) = \frac{V_{ki}(z, \mathbf{x})}{\varphi V_{nk}(z, \mathbf{x})} \leq 1 \quad (25)$$

where P_n is the required axial strength; P_i is the peak value of axial force due to gravity loads for the i -th wind load realization; M_{nx} and M_{ny} are the nominal flexural strengths about the x and y axes; V_{nk} is the nominal shear strength; M_{xi} and M_{yi} are the peak bending moments; V_{ki} is the peak shear force and $\varphi = 0.9$ is a commonly-employed capacity reduction factor. Fragility functions are defined as a function of DCIs. The previous equations are adapted from the AISC Design Standard (2017), where the maximum moments and axial forces, $M_{xi}(\mathbf{x})$, $M_{yi}(\mathbf{x})$ and $P_i(\mathbf{x})$ are found directly from the extreme wind load analysis (not requiring load multiplication factors). For the sake of simplicity, z in Eqs (22) - (25) refers to each column located

at z .

Type 4 are direct losses related to the TMDs' stroke limit crossing. Indeed, when the maximum allowable TMD displacement is reached, an impact between the TMD mass and the substructure occurs that reduces the performance of the control system and can produce damage to the control device as well as to the structural system. The DCI index, in this case, is defined as

$$DCI_{TMD,ki} = \frac{\delta_{ki}}{v\delta_{nk}} \quad (26)$$

where δ_{nk} is the stroke threshold of the TMD in the direction k ($\delta_{nx} = \delta_{ny} = 1.2$ m, which is a common threshold value for TMDs available in the market), δ_{ki} is the peak stroke of the TMD for the i -th wind load realization and v is a "partial safety factor" that keeps the stroke sufficiently far from the threshold ($v=0.9$). Fragility functions are defined in terms of DCI_{TMD} .

Finally, type 5 are indirect losses related to business downtime due to occupants' discomfort. The fragility curve is a function of the peak acceleration computed using Eq. (7b).

5. Application to a case study

5.1 Preliminary design of structural and nonstructural elements

The application example focuses on a steel tall building, 180 m high, having square floor section with side lengths $B=D=30$ m. The structural system is composed of columns, central square core made of steel beams and bracings, beams and peripheral outriggers in both principal lateral directions at three levels along the height (Venanzi, 2015). A preliminary design was carried out using a full 3D finite element model of the building and adopting static-equivalent vertical and lateral loads, derived from American standard prescriptions (ASCE/SEI 7-16 2017). Columns have hollow square cross sections with dimensions gradually decreasing every ten stories along the building height. The column dimensions are reported in Table 2 where t_s is the outside side length, t_{wt} is the wall thickness. A system of steel columns, beams and cross-braces with hollow rectangular cross-section constitutes the internal core. The floor system is composed of 0.2 m thick concrete slabs supported by I-shaped steel beams having overall section height $t_{-3}=0.26$ m, top flange width $t_{-2}=0.14$ m, top flange thickness $t_f=9.8e-03$ m, web thickness $t_w=6.4e-03$ m, bottom flange width $t_{b6}=0.14$ m and bottom flange thickness $t_{fb}=9.652e-03$ m

For the purpose of the optimization procedure, a simplified dynamic model of the system with three degrees of freedom per floor is utilized, reproducing the behavior of the first three fundamental structural modes extracted from the full 3D model of the building. The first two modes are uni-planar horizontal-translational and the third one is torsional. Power-law vibration mode shape functions are used in the numerical simulations. Table 3 shows the first three natural frequencies and power-law exponents of the

Table 2 Main dimensions of the column cross-sections at various floors

Floors	t_{-2} [m]	t_{-wt} [m]
1-20	0.9	0.07
21-40	0.8	0.06
41-60	0.7	0.05

Table 3 Fundamental natural frequencies (n_k), damping ratios (ξ_k) and power law exponents (γ_k) of the tall building case study

Mode	n_k (Hz)	ξ_k (%)	γ_k
1	0.210	0.01	1.12
2	0.210	0.01	1.12
3	0.247	0.01	0.86

vibration modes [$\Phi_k(z) = (z/H)^{\gamma_k}$ with $k=x,y$ and $\Phi_\psi(z) = (z/H)^{\gamma_\psi}$].

The considered control system is composed of two unidirectional TMDs, located at the elastic center of the top floor of the building (also coincident with the mass center). As a first step before optimization, the mass ratio is assumed equal to $\mu=2\%$ in both principal directions. The parameters of the TMDs are tuned to control the response of the first two lateral modes. The Warburton relationships (Warburton 1982) are adopted to compute the optimal stiffness and damping coefficient of the TMDs.

5.2 Wind load modeling and structural analysis

Wind loads are obtained from experimental data recorded in the wind tunnel (Simiu and Yeo 2015). Wind tunnel tests were carried out at the Inter-University Research Center for Building Aerodynamics and Wind Engineering (CRIACIV, Prato, Italy) on a rigid model equipped with 120 pressure taps, 30 on each vertical face, equally divided into 5 levels (Venanzi and Materazzi, 2012). The geometric scale of the model is 1:500. The wind tunnel roughness corresponds to suburban terrain whose wind speed profile is properly described by a power-law function with exponent approximately equal to 0.23. Pressures are measured for different mean wind incidence angles (θ), between 0° and 360° with 22.5° step increments. The 30 s long wind tunnel pressure records, whose duration is equivalent to approximately 1.5 hours at full scale, are divided into 8 segments (realizations i), having a duration corresponding to 10 min at full scale.

Generalized loads (Eq. (3)) are computed by integrating pressure time histories over the model's surface.

In order to compute the failure probability, Eq. (9), it is necessary to obtain the joint probability density function $f(V_{ref}, \theta)$. As detailed in Ierimonti *et al.* (2017b), it is assumed that V_{ref} and θ are independent, as a first approximation, i.e., $f(V_{ref}, \theta) = f(V_{ref})f(\theta)$. The building is located near Boston (Massachusetts, USA). Data of wind direction available from an online database (NERACOOS), relative to meteorological measurements from a weather station in the Boston area, are used to compute $f(\theta)$. The PDF of the annual maxima of the mean-wind speed $f(V_{ref})$ at

the reference roof-top elevation $H=180$ m is numerically reconstructed from information extracted from the American standard prescriptions (ASCE-7 2016, Ierimonti *et al.* 2017).

The EDPs are the inter-story drift ratio (*IDR*) (Eq. (21)), the peak floor acceleration (a) corresponding to the maximum absolute value of the peak response (Eq. (7b)), the demand-to-capacity index for bending and axial force (DCI_{MN}), the one for shear (DCI_V) and the one for the TMDs maximum stroke (Eqs. (24) - (26)). EDPs are computed for each one of the 8 force time histories segments through frequency domain analysis, as detailed in Eqs. (3) - (8), and for each column at the floor level. The probability density function of the EDPs $f(EDP | V_{ref}, \theta, CS)$ is computed from the results of the 8 analyses, by assuming a lognormal distribution with mean value and standard deviation obtained from the 8 output samples.

Prior to the wind load analysis, the following load combinations provided by ASCE 7-16 (Standards ASCE/SEI 7-16 2017) are adopted for preliminary maximum strength design and for the evaluation of damage-to-capacity indices (Eqs. (24) - (26))

$$\begin{aligned} 1.2D + 1.0W + 1.0L \\ 1.0D + 1.0W \end{aligned} \quad (27)$$

5.3 Fragility modeling

All the types of damage presented in Section 4, related to nonstructural elements, structural elements, TMDs and business downtime are considered in the numerical simulations.

The considered nonstructural elements (Type 1), uniformly distributed over the floors, are glass façades (drift-related damage), partition walls (drift-related damage) and suspended ceilings (acceleration-related damage). Empirical fragility curves for the considered nonstructural elements are derived from the FEMA (Federal Emergency Management Agency) on-line database (FEMA-P-58 2012), as previously done by several Authors (Chuang & Spence 2017, Ierimonti *et al.* 2017). Fragility curves are referred to unit elements: 100 linear feet (about 30 m) for the partition walls, 2500 square feet (about 230 square meters) for the suspended ceilings and a 1.8 m high panel with an aspect ratio of 6:5 for glass façades. The considered structural elements (Type 2) are the columns at each floor of the building. The unit element is the single column of each floor. The damage to the TMDs due to the stroke limit crossing (Type 3) is related to DCI_{TMD} . For the quantification of the annual damage probability associated with a revenue loss due to business downtime (Type 4), the peak acceleration $a(z)$, evaluated through Eq. (7b), is selected as *EDP*. The mean value of the Type 4 losses is chosen as the common accepted average value of the perceptibility threshold, i.e., 10 milli-g (Burton *et al.* 2015, Griffis 1993, Chang 1973).

Type 1, Type 2, Type 3 and Type 4 fragility functions are assumed as lognormally distributed, whose mean values and standard deviations are summarized in Table 4.

Table 4 Fragility curve characteristics: mean values and standard deviations

	Glass façades	Partition walls	Suspended ceilings	DCI_{MN}	DCI_{TMD}	Business downtime
Mean	0.0156	0.0035	0.25	1	1	10 μ g
Standard deviation	0.35	0.7	0.4	0.1	0.1	0.1 μ g

5.4 Cost modeling

The initial construction cost of the structure is assumed as a percentage of the total mass $M(\mathbf{x})$ of the structure

$$C_{0s}(\mathbf{x}) = c_{0s}M(\mathbf{x}) \quad (28)$$

with $c_{0s}=1.07$ (Hasançebi 2017, Ierimonti *et al.* 2018). The initial construction cost of the TMDs is defined as

$$C_{0cs}(\mathbf{x}) = c_{0cs}m(\mathbf{x}) \quad (29)$$

where $c_{0cs}=1.077$ (Wang *et al.* 2016) and m is the mass of the TMD.

Maintenance costs of the structure are defined as

$$C_m = \alpha_m C_{0s} \quad (30)$$

with $\alpha_m=0.01$. The maintenance costs of the TMD are included in their initial cost C_{0cs} (Wang *et al.* 2016).

Repair costs referred to nonstructural unit elements, C_r^f , are taken from FEMA-P-58 (2012). The lower bound for the unit repair costs, suggested by FEMA-P-58 (2012) for each nonstructural element, is usually adopted when a large number of elements must be repaired, while the upper one is utilized when a limited number of elements must be repaired. In the present application, the lower bounds are chosen due to the large number of elements potentially involved. The unit costs are reported in Table 5. Repair cost for structural unit elements are assumed equal to the initial cost of unit elements, expressed by

$$C^r(\mathbf{x}) = c_r \Gamma(\mathbf{x}) \quad (31)$$

where $\Gamma(\mathbf{x})$ is the weight of the single steel element and c_r is the cost per unit weight of the steel element, reported in Table 5. Repair cost that is needed when the TMDs limit stroke is exceeded, is defined as a function of the TMD mass, m

$$C^r(\mathbf{x}) = c_{TMD,r} m(\mathbf{x}) \quad (32)$$

where the coefficient $c_{TMD,r}$ is shown in Table 5.

The unit cost related to business downtime (C_{IL}) that pertains to the single floor level, is evaluated as follows

$$\hat{C}_{IL}(\mathbf{x}, z) = \kappa(z) C_{IL} / n_{floors} \quad (33)$$

where $\kappa(z)$ is a coefficient that modifies the unit cost according to the designated use of the floor at height z , C_{IL} is the average total unit cost, and n_{floors} is the number of floors of the building. The average cost C_{IL} of a unit time of downtime (one hour) is obtained from data by the Information Technology Intelligence Consulting (ITIC, 2016) and it is reported in Table 5, under the hypothesis that the arrival time of a windstorm causes one hour of business interruption.

Table 5 Reference-element unit costs

Glass façades C^r [\$]	Partition walls C^r [\$]	Suspended ceilings C^r [\$]	Structural members c_r	TMD $c_{TMD,r}$	Business downtime C_{IL} [\$]
1700	2200	3300	0.01	0.007	100000

6. Integrated optimal design of the case study tall building

6.1 Parametric analyses

To investigate the effect of the design variables on the expected cost, parametric analyses are carried out by varying μ and α . The mass ratio μ is varied between 0.005 and 0.04 with 0.005 step increments, while the coefficient α is varied from 0.6 to 1.4. Figs. 2 and 3 report the disaggregated cost components, obtained from the parametric analyses. Results are expressed in terms of expected life-cycle costs at $t=100$ years and normalized to the initial construction cost (sum of the cost of the structure and the TMDs). Inspection of the figures suggests that the expected cost has minimum values for higher values of μ and α . This trend is more evident for glass façades Fig. 2(a), suspended ceilings Fig. 2(c), columns Fig. 3(a) and TMD stroke limit crossing Fig. 3(b).

Moreover, in order to analyze, for each component, the influence of μ and α , the percentage variations between the maximum and the minimum values of the expected cost within the investigated range of variation of μ and α are reported in Tables 6 and 7.

Sensitivity analysis results allow to identify which type of loss is more influenced by the variation of the design variables, as follows

- glass façades are the most sensitive to the damage with variations higher than 1, especially as a function of α (Table 6). These results are consistent with Fig. 2(a) since a more flexible structure ($\alpha < 1$) with a small value of the TMD mass ratio ($\mu=0.005$) can cause large inter-story displacements.
- Partition walls are more sensitive to the variation of α with a maximum variation equal to about 2.2, while different TMD mass ratios do not significantly affect the cost with a maximum variation of 0.6.
- Suspended ceilings have approximately the same variations in terms of expected costs with respect to both parameters.
- Columns are more sensitive to the variation of α with respect to the TMD mass ratio μ , with a variation of about 4.
- TMD is more sensitive to the variation of mass ratio μ , especially for the lower values of μ , with respect to the variation of α .
- Business downtime does not appear to significantly change in terms of expected costs with respect to both parameters. This result is probably due to the effectiveness of the control system in reducing structural vibrations in an adaptive manner and it is certainly affected by the selected threshold for the human perception of accelerations (Sect 5.3.) and by the adopted cost model.

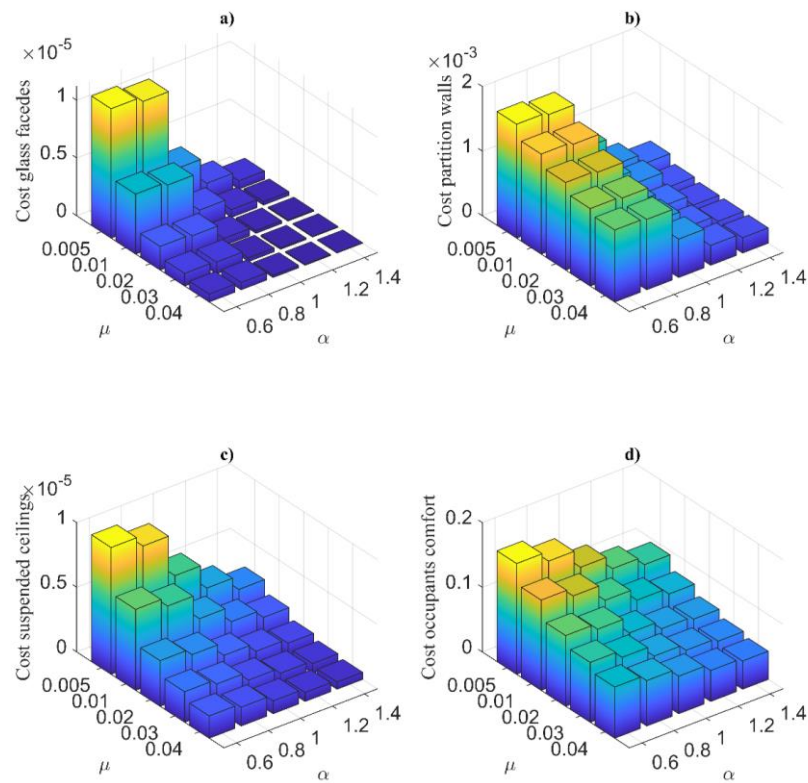


Fig. 2 Normalized expected life-cycle cost obtained by varying μ and α for: (a) glass façades, (b) partition walls, (c) suspended ceilings, (d) business downtime

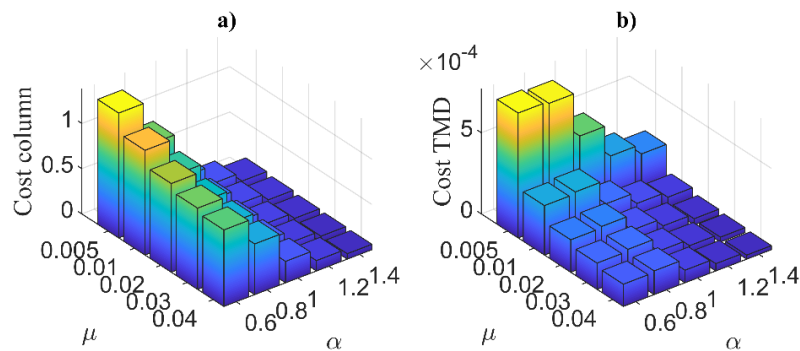


Fig. 3 Normalized expected life-cycle cost obtained by varying μ and α for: (a) column failure, (b) TMD stroke limit crossing

Table 6 Percentage cost variation (between maximum and minimum values) for different values of α

Type of loss	Damaged elements	$\Delta_{\mu,\alpha=0.8}$	$\Delta_{\mu,\alpha=0.90}$	$\Delta_{\mu,\alpha=1}$	$\Delta_{\mu,\alpha=1.1}$	$\Delta_{\mu,\alpha=1.2}$
Direct/non-structural	Glass façades	14.77	16.76	19.74	22.29	24.71
Direct/non-structural	Partition walls	3.47	4.52	4.53	3.94	3.72
Direct/non-structural	Suspended ceilings	2.54	2.40	2.25	2.18	2.15
Direct/structural	Columns	12.10	12.31	12.72	13.08	13.35
Direct/structural	TMD	2.40	3.71	4.29	4.46	4.57
Indirect/comfort related	Business downtime	0.83	0.91	0.86	0.87	0.82

Table 7 Percentage cost variation (between maximum and minimum values) for different values of μ

Type of loss	Damaged elements	$\Delta_{\mu=0.005,\alpha}$	$\Delta_{\mu=0.01,\alpha}$	$\Delta_{\mu=0.015,\alpha}$	$\Delta_{\mu=0.02,\alpha}$	$\Delta_{\mu=0.04,\alpha}$
Direct/non-structural	Glass façades	15.31	16.12	19.30	22.80	25.61
Direct/non-structural	Partition walls	0.56	0.56	0.65	0.79	0.65
Direct/non-structural	Suspended ceilings	4.63	5.14	4.75	4.51	4.01
Direct/structural	Columns	0.61	0.59	0.68	0.75	0.76
Direct/structural	TMD	4.56	4.12	5.16	5.36	8.09
Indirect/comfort related	Business downtime	1.14	1.2	1.17	1.20	1.13

Table 8 Results of the integrated optimization in terms of design variables and objective function for different lifetime durations and different weights of the objective function

		$t = 10$ yrs			$t = 30$ yrs			$t = 50$ yrs			$t = 70$ yrs		
p_1	p_2	α	μ	Z									
1	1	1.397	0.040	3.75E7	1.395	0.040	4.14E7	1.399	0.039	4.28E7	1.395	0.040	4.34E7
1	5	1.394	0.040	4.30E7	1.388	0.040	5.22E7	1.397	0.039	5.56E7	1.388	0.040	5.68E7
1	10	1.388	0.040	4.98E7	1.281	0.038	7.44E7	1.397	0.039	7.16E7	1.355	0.039	7.74E7
5	1	0.787	0.030	1.75E8	0.908	0.036	1.92E8	0.918	0.038	1.98E8	0.921	0.040	2.00E8
10	1	0.610	0.020	3.28E8	0.612	0.040	3.62E8	0.801	0.037	3.83E8	0.790	0.040	3.81E8

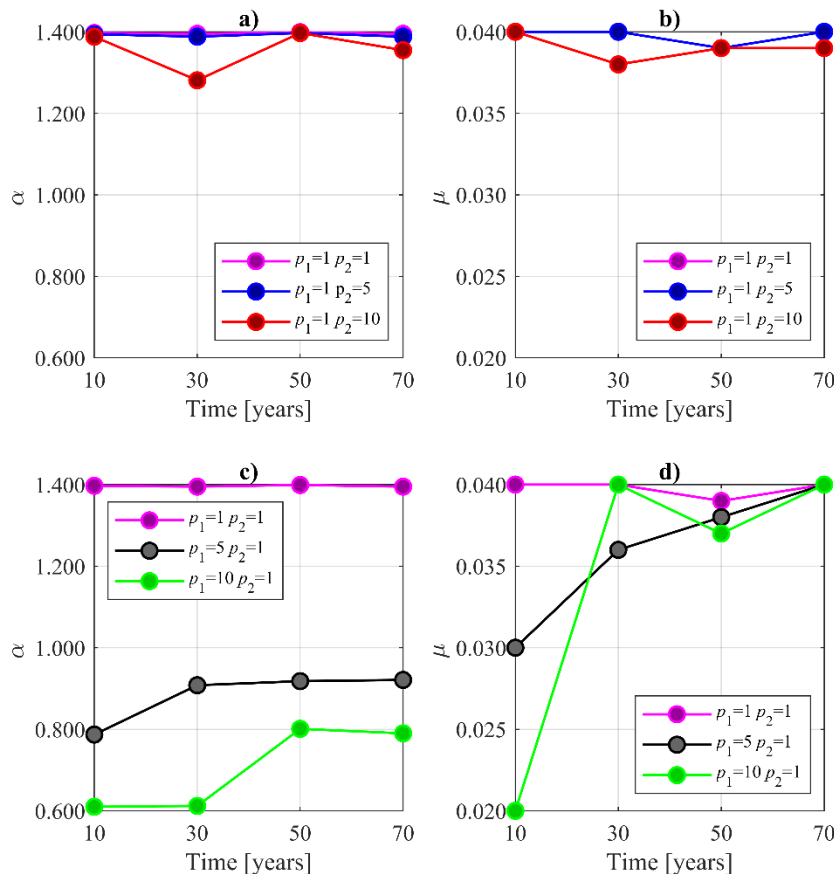


Fig. 4 Design variables as a function of lifetime (years) for different sets of p_1 and p_2 : a)-c) α ; b)-d) μ

6.2 Results of the optimization procedure

The integrated optimization has been carried out for the tall building case study. Preliminarily, the global stiffness and mass matrices sets, obtained from the parametric analyses presented in Section 5.1, are collected into a database to which the optimization algorithm can tap into. Indeed, for each trial value of the design variables, the corresponding global stiffness and mass matrices are used for structural analysis.

Results are presented in Table 8 in terms of design variables (α , μ) and objective function (Z) for different lifetime durations (10, 30, 50 and 70 years) and different weights (p_1 and p_2) of the two terms of Z , the one related to initial costs and the one related to lifetime losses.

Results of optimal design carried out for $t=10$ years show that as the weight of the term related to initial costs p_1 increases, the coefficients α and μ decrease, since the optimization procedure leads to a solution with minimum initial cost. Conversely, if the weight of the term related to lifetime losses p_2 is greater than or equal to p_1 , the optimal parameters are close to the upper bounds of the design space ($\alpha=1.4$ and $\mu=0.04$). This trend is also confirmed for greater lifetime durations, although a limited increment in the optimal values of the design variables is observed with the increase of lifetime duration.

Fig. 4 shows the optimal values of the design variables (α , μ) as a function of the lifetime duration, obtained for the different sets of p_1 and p_2 reported in Table 8. In particular, Figs. 4(a) - 4(b) show the results for $p_2 \geq p_1$ and Figs. 4(c) -

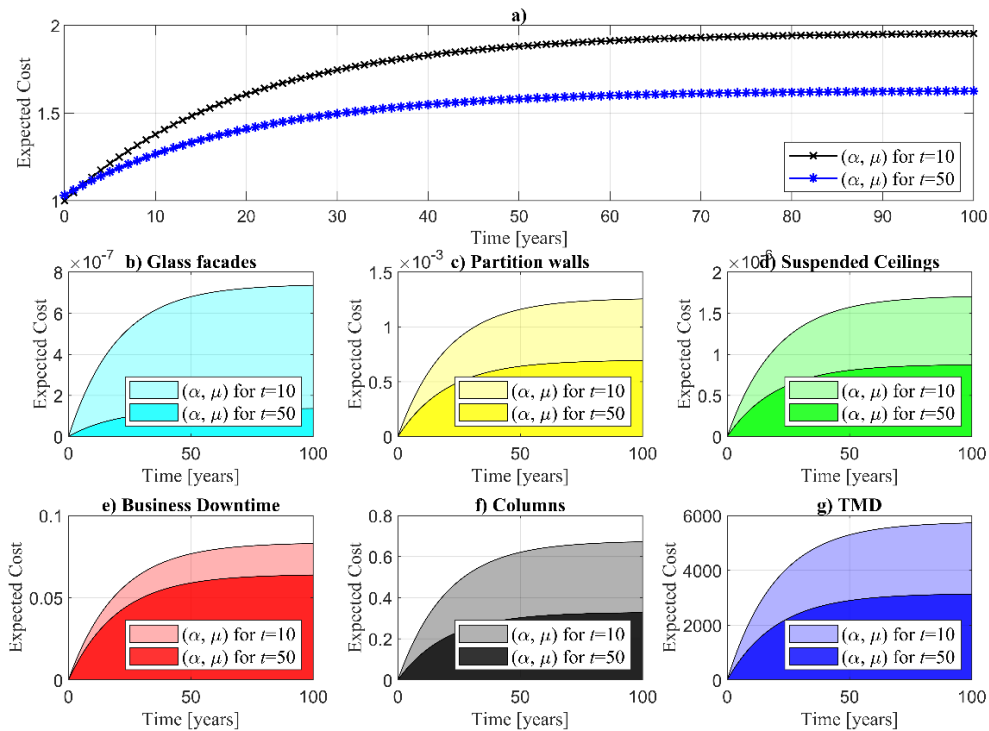


Fig. 5 Aggregated and disaggregated expected Life-Cycle Costs over time for the values of the design variables α and μ optimized for $t=10$ years and $t=50$ years

Table 9 Initial construction costs C_{0s} and initial TMD cost C_{0cs} (US dollars \$) as a function of the design variables optimized for $t=10$ years and $t=50$ years

	C_{0s} [10^7]	C_{0cs} [10^5]
(α, μ) for $t = 10$ yrs	3.0	3.2
(α, μ) for $t = 50$ yrs	3.2	4.4

4(d) show the results for $p_1 \geq p_2$. If p_2 is greater than p_1 , the term of the objective function related to repair costs and indirect losses has a predominant effect on the total costs compared to the terms related to initial costs. Therefore, the design variables assume values close to their upper bounds. If $p_1 \geq p_2$, the term of the objective function related to the initial costs has greater influence on total costs. For $t=10$ years, the design variables assume values close to their lower bounds while, for $t > 10$ years, they increase with the lifetime duration to reduce the costs associated with serviceability and ultimate limit states.

Fig. 5 shows the aggregated and disaggregated expected life-cycle costs obtained using the values of α and μ optimized for $t=10$ and $t=50$ years. In particular, Fig. 5(a) shows the total expected life-cycle costs and Figures 5(b) - 5(g) separately illustrate the disaggregated expected life-cycle cost components for the different limit states. The expected costs are normalized with respect to the initial cost of the structure and the TMDs corresponding to the optimal values of the design variables for $t=10$ years. As expected, optimizing the parameters α and μ considering a reference time $t=10$ causes an overall cost increase over time, while the adoption of the solution obtained for $t=50$ years, leads to higher initial cost (Table 9) but also to a significant reduction of expected life-cycle costs (Fig. 5(a)).

Optimization results shown in Figs. 5(b) - (g) are strongly non-linear and dependent on the lifetime chosen to compute the cost-related objective function. For the specific structural model and cost model adopted in this application, the most significant losses are those related to the failure of columns and those related to business downtime due to occupants' discomfort.

7. Limitations and future work

The results presented in Section 5 demonstrated the effectiveness of the proposed methodology in achieving the integrated optimal design of the structure and the TMDs. Nonetheless, it is necessary to point out that the framework is based on assumptions that can limit its practical implementation and should be considered to obtain results entirely usable for real applications.

One simplified assumption regards the structural modeling and analysis. Three uncoupled modal contributions are considered for the evaluation of the structural response. In the cases of complex structural shapes, it may be necessary to consider coupling between the modes by including the generalized, modal cross spectra in the computation of the response power spectral densities.

Another simplification has been adopted for the design variables definition. A unique coefficient α is selected as design variable, that multiplies the nominal values of the structural elements' thickness. This implies that the relationships between strength at different floors have been set by a preliminary analysis. Another option is to differentiate the weight coefficients at various floors.

Similarly, the mass ratio μ is assumed equal for the two TMDs but in general, when the structure has different stiffness in the two principal lateral directions, it can be appropriate to incorporate explicitly μ_x and μ_y among the design variables.

Another important assumption regards the evaluation of costs related to failure of structural elements and nonstructural elements. The determination of the internal forces in the columns is carried out adopting the shear type hypothesis but, especially in the case of buildings with coupled wall-frame systems, a more rigorous internal force analysis must be carried out. This could be done, for example, by using influence functions (Venanzi *et al.* 2006) that reproduce the effect of unit forces or displacements applied at different levels of the structure. Moreover, the failure probability of structural and nonstructural elements is computed at a reference location, while in order to provide a more rigorous computation, the specific location of each element over the floor should be considered.

It is also necessary to remark that the specific fragility and cost models adopted may significantly influence the results. As, to the Authors' knowledge, fragility curves for non-structural components of tall buildings subjected to wind loads are still not available, fragility curves have been derived from seismic FEMA standard. Fragility curves for structural elements and business downtime are evaluated by assuming a lognormal distribution and a suitable value of the standard deviations. The definition of the fragility models must be carefully reconsidered before using the procedure in practical applications. Similarly, the cost model can be adapted to the specific building design.

Other simplified assumptions regard the wind load characterization. It is assumed in the proposed formulation that the reference mean wind speed and the mean wind direction are independent random variables. This assumption is acceptable in the case of coastal regions and extra-tropical synoptic winds, marginally affected by tropical storms such as hurricanes, but in regions where hurricanes are likely to land ashore, the two variables are inter-connected (Cui and Caracoglia 2018) and it is necessary to consider the mutual dependence of the two factors. Moreover, the use of HFFB (rigid) models, tested in wind tunnel, may become inadequate when super-tall building or towers are considered, since aeroelastic effects due to wake excitation may influence the estimation of the effective damping of the structure. This issue may be circumvented by supplementing HFFB or pressure integration tests with aeroelastic tests. Furthermore, the frequency domain usually acceptable for extra-tropical storms and hurricanes becomes inadequate for the central regions of the United States, where damage is often associated with nonstationary, meso-scale wind events, such as thunderstorm downbursts. In this case (Le and Caracoglia 2018), either time-domain integration methods or the wavelet-Galerkin numerical method are necessary for the solution of the dynamic equations and the damage probability.

Future work should possibly include generalization of the proposed optimization algorithm, accounting for the simplified assumptions indicated above. Furthermore, analysis of the downtime effects should also include indirect business losses due to extended loss of operations. Finally, the intervention cost analysis should possibly

consider the cumulative cost associated with multiple building structures in a whole community, i.e. in the context of community and urban resilience studies, accounting for the mutual correlation (or partial correlation) of the hazard curves (reference wind speed and direction – an issue in hurricane prone-regions) and the correlation of the fragility functions in an urban setting; in fact, building materials and building construction types may be similar for nearby buildings.

8. Conclusions

A life-cycle cost-based optimization framework was proposed for the integrated design of wind-excited tall buildings, equipped with Tuned Mass Dampers (TMD). The procedure attempts the simultaneous optimization of structural sections and mass ratio of the TMDs, by minimizing a functional comprising initial costs of the structure and the control system, and intervention costs related to repair, maintenance and business downtime for the whole structural lifetime. Both serviceability and ultimate limit states related to the structural members, the main non-structural components, the TMD damage and the occupants' discomfort are employed for the computation of repair costs. The selected case study is a simplified tall building structure, equipped with TMDs in two orthogonal directions. Initial parametric analyses enabled investigating the influence of the variation of the design parameters on the disaggregated expected intervention costs. The optimization was carried out for different values of the coefficients weighting the initial cost and the repair costs, demonstrating the efficiency of the procedure for the integrated design of the structure and the control system.

Acknowledgments

This collaborative research activity was initiated as part of Laura Ierimonti's study period at Northeastern University in 2016. This activity was supported by the University of Perugia, Italy within the framework of the International PhD program between the Universities of Perugia, Florence and TU Braunschweig.

Luca Caracoglia would like to acknowledge the support of the National Science Foundation (NSF) of the United States of America, CAREER Award CMMI-0844977 in 2009-2014, and the partial support of NSF Award CMMI-1434880 in 2014-2018. Luca Caracoglia also acknowledges the support of the University of Perugia, mobility program for visiting professors in 2015 ("Decreto Rettoriale" D.R. 2244, 2014). Any opinions, findings and conclusions or recommendations are those of the authors and do not necessarily reflect the views of the sponsors.

References

AISC Steel Construction Manual (2017), American Institute of Steel Construction, Illinois, USA.

- Aly, A.M. (2015), "Control of wind-induced motion in high-rise buildings with hybrid TM/MR dampers", *Wind Struct.*, **21**(5), 565-595. <https://doi.org/10.12989/was.2015.21.5.565>.
- ASCE/SEI 7-16 (2017), "Minimum Design Loads and Associated Criteria for Buildings and Other Structures", American Society of Civil Engineers.
- Bashor, R. and Kareem, A. (2007), "Probabilistic performance evaluation of buildings: an occupant comfort perspective", *Proceedings of the 12th International Conference on Wind Engineering*.
- Bernardini, E., Spence, S.M. and Kareem, A. (2013), "A probabilistic approach for the full response estimation of tall buildings with 3d modes using the HFFB", *Struct. Safety*, **44**, 91-101. <https://doi.org/10.1016/j.strusafe.2013.06.002>.
- Burton, M., Kwok, K. and Abdelrazaq, A. (2015), "Wind-induced motion of tall buildings: designing for occupant comfort", *Int. J. High-Rise Build.*, **4**(1), 1-8. <https://doi.org/10.21022/IJHRB.2015.4.1.001>.
- Chang, F.K. (1973), "Human response to motions in tall buildings", *J. Struct. Division*, **499**(6), 1259-1272.
- Chen, X., Kwon, D.K. and Kareem, A. (2014), "High-frequency force balance technique for tall buildings: A critical review and some new insights", *Wind Struct.*, **18**(4), 391-422. <http://dx.doi.org/10.12989/was.2014.18.4.391>.
- Chuang, W.C. and Spence, S.M. (2017), "A performance-based design framework for the integrated collapse and non-collapse assessment of wind excited buildings", *Eng. Struct.*, **150**, 746-758. <https://doi.org/10.1016/j.engstruct.2017.07.030>.
- Ciampoli, M. and Petrini, F. (2012), "Performance-based Aeolian risk assessment and reduction for tall buildings", *Probabilistic Eng. Mech.*, **28**, 75-84. <https://doi.org/10.1016/j.probenmech.2011.08.013>.
- Cornell, C. and Krawinkler, H. (2000), "Progress and challenges in seismic performance assessment", *PEER Center News*, **3**(2), 1-3.
- Cui, W. and Caracoglia, L. (2018), "A unified framework for performance-based wind engineering of tall buildings in hurricane-prone regions based on lifetime intervention-cost estimation", *Struct. Safety*, **73**, 75-86. <https://doi.org/10.1016/j.strusafe.2018.02.003>.
- Davenport, A.G. (1964), "Note on the distribution of the largest value of a random function with application to gust loading", *Proc. Inst. Civil. Eng.*, **28**, 187-196. <https://doi.org/10.1680/icep.1964.10112>.
- Davenport, A.G. (1967), "Gust loading factors", *J. Struct. Division*, ASCE, **93**, 11-34.
- EN 1991-1-4:2005 (2005), "Eurocode 1: actions on structures - part 1-4: general actions - wind actions", European Committee for Standardization.
- FEMA-P-58 (2012), "Performance assessment calculation tool, volume 1", <http://www.fema.gov/media-library/assets/documents/90380>.
- Griffis, L. (1993), "Serviceability limit states under wind load", *Eng. J. Ame. Institute Steel Construct.*, **30**, 1-16.
- Hasançebi, O. (2017), "Cost efficiency analyses of steel framework for economical design of multi-storey buildings", *J. Construct. Steel Res.*, **128**, 380-396. <https://doi.org/10.1016/j.jcsr.2016.09.002>.
- Holmes, J., Rofail, A. and Aurelius, L. (2003), "High frequency base balance methodologies for tall buildings with torsional and coupled resonant modes", *Proceedings of the 11th International Conference on Wind Engineering*, U.S.A.
- Huang, M.F., Tse, K.T., Chan, C.M. and Lou, W.J. (2011), "Integrated structural optimization and vibration control for improving wind-induced dynamic performance of tall buildings", *Int. J. Struct. Stab. Dyn.*, **11**(6), 1139-1161. <https://doi.org/10.1142/S021945541100452X>.
- Ierimonti, L., Caracoglia, L., Venanzi, I. and Materazzi, A.L. (2017), "Investigation on life-cycle damage cost of wind-excited tall buildings considering directionality effects", *J. Wind Eng. Indus. Aerod.*, **171**, 207-218. <https://doi.org/10.1016/j.jweia.2017.09.020>.
- Ierimonti, L., Venanzi, I. and Caracoglia, L. (2018), "Life-cycle damage-based cost analysis of tall buildings equipped with tuned mass dampers", *J. Wind Eng. Indus. Aerod.*, **176**, 54-64. <https://doi.org/10.1016/j.jweia.2018.03.009>.
- Ierimonti, L., Venanzi, I., Caracoglia, L. and Materazzi, A.L. (2019), "Cost-based design of nonstructural elements for tall buildings under extreme wind environments", *J. Aeros. Eng. ASCE*, **32**(3), 04019020. [https://doi.org/10.1061/\(ASCE\)AS.1943-5525.0001008](https://doi.org/10.1061/(ASCE)AS.1943-5525.0001008).
- ITIC (2016), "Cost of Hourly Downtime Soars: 81 % of Enterprises Say it Exceeds \$ 300K On Average" <http://itic-corp.com/blog/2016/08/cost-of-hourly-downtime-soars-81-ofenterprises-say-it-exceeds-300k-on-average/>.
- Kareem, A., Kijewski, T. and Tamura, Y. (1999), "Mitigation of motions of tall buildings with specific examples of recent applications", *Wind Struct.*, **2**(3), 201-251.
- Kunnath, S. (2006), "Application of the PEER PBEE Methodology to the I-880 Viaduct", *Report No. 2006/10*, University of California, Davis, U.S.A.
- Kwok, K.C.S., Burton, M.D. and Abdelrazaq, A.K. (2015), "Wind-induced motion of tall buildings: Designing for habitability", *Ame. Soc. Civil Eng. (ASCE)*, 1-66. <https://doi.org/10.1061/9780784413852>.
- Le, V. and Caracoglia, L. (2019), "Computationally efficient stochastic approach for the fragility analysis of vertical structures subjected to thunderstorm downburst winds", *Eng. Struct.*, **176**, 152-169. <https://doi.org/10.1016/j.engstruct.2018.03.007>.
- NERACOOS (2017), "Northeastern regional association of coastal and ocean observing systems, <http://www.neracoos.org>.
- Palmeri, A., Ricciardelli, F., Muscolino, G. and De Luca, A. (2004), "Effects of viscoelastic memory on the buffeting response of tall buildings", *Wind Struct.*, **7**(2), 89-106. <https://doi.org/10.12989/was.2004.7.2.089>.
- PEER-TBI (2010), "Tall buildings initiative, guidelines for performance-based seismic design of tall buildings", *Report No. 2010/05, TBI Guidelines Working Group*, PEER Center, University of Berkeley, California, U.S.A.
- Pozzuoli, C., Bartoli, G., Peil, U. and Clobes, M. (2013), "Serviceability wind risk assessment of tall buildings including aeroelastic effects", *J. Wind Eng. Ind. Aerod.*, **123**, 325-38. <https://doi.org/10.1016/j.jweia.2013.09.014>.
- Qisheng, L., Hong, C., Guiqing, L., Shujing, L. and Dikai, L. (1999), "Optimal design of wind-induced vibration control of tall buildings and high rise structures", *Wind Struct.*, **2**(1), 69-83. <https://doi.org/10.12989/was.1999.2.1.069>.
- Ricciardelli, F. (1999), "Linear model for structures with tuned mass dampers", *Wind Struct.*, **2**(3), 151-171. <https://doi.org/10.12989/was.1999.2.3.151>.
- Ross, A.S., El Damatty, A.A. and El Ansary, A.M. (2015), "Application of tuned liquid dampers in controlling the torsional vibration of high rise buildings", *Wind Struct.*, **21**(5), 537-564. <http://dx.doi.org/10.12989/was.2015.21.5.000>.
- Said, E. and Matsagar, V. (2018), "Wind response control of tall buildings with a tuned mass damper", *J. Build. Eng.*, **15**, 51-60. <https://doi.org/10.1016/j.job.2017.11.005>.
- Simiu, E. (2011), "Design of buildings for wind: A guide for ASCE 7-10 standard users and designers of special structures", John Wiley & Sons, Inc., New Jersey, U.S.A.
- Simiu, E. and Yeo, D. (2015), "Advances in the design of high-rise structures by the wind tunnel procedure: Conceptual framework", *Wind Struct.*, **21**(5), 489-503. <http://dx.doi.org/10.12989/was.2015.21.5.489>.

- Sivanandam S. and Deepa S. (2008), "Genetic Algorithm Optimization Problems. In: Introduction to Genetic Algorithms". Springer, Berlin, Germany.
- Tallin, A. and Ellingwood, B. (1985), "Analysis of torsional moments on tall buildings", *J. Wind Eng. Indus. Aerod.*, **18**(2), 191-195. [https://doi.org/10.1016/0167-6105\(85\)90097-2](https://doi.org/10.1016/0167-6105(85)90097-2).
- Tse, K.T., Yu, X.J. and Hitchcock, P.A. (2014). "Evaluation of mode-shape linearization for HFBB analysis of real tall buildings", *Wind Struct.*, **18**(4), 423-441. <http://dx.doi.org/10.12989/was.2014.18.4.423>.
- Venanzi, I. (2015), "Robust optimal design of tuned mass dampers for tall buildings with uncertain parameters", *Struct. Multidiscip. O.*, **51**, 239-250. <https://doi.org/10.1007/s00158-014-1129-4>.
- Venanzi, I. and Materazzi, A.L. (2012). "Acrosswind aeroelastic response of square tall buildings: a semi-analytical approach based on wind tunnel tests on rigid models", *Wind Struct.*, **15**(6), 495-508.
- Venanzi, I. Fritz, W.P. and Simiu, E. (2006). "A database-assisted design approach for the assessment of wind induced torsional effects on tall buildings", *Proceedings of the Structures Congress and Exposition*.
- Venanzi, I., Lavan, O., Ierimonti, L. and Fabrizi, S. (2018), "Multi-hazard loss analysis of tall buildings under wind and seismic loads", *Struct. Infrastruct. Eng.*, **14**(10), 1295-1311. <https://doi.org/10.1080/15732479.2018.1442482>.
- Wang, L., Zhao, X. and Zheng Y.M. (2016), "A combined tuned damper and an optimal design method for wind-induced vibration control of super tall buildings", *Struct. Des. Tall Spec. Build.*, **25**(10), 468-502. <https://doi.org/10.1002/tal.1268>.
- Warburton, G. (1982), "Optimum absorber parameters for various combination of response and excitation parameters", *Earthq. Eng. Struct. Dyn.*, **10**(3), 381-401. <https://doi.org/10.1002/eqe.4290100304>.
- Wen, Y.K. and Kang, Y.J. (2001), "Minimum building life-cycle cost design criteria. I: Methodology", *J. Struct. Eng.*, **127**(3), 330-337. [https://doi.org/10.1061/\(ASCE\)0733-9445\(2001\)127:3\(330\)](https://doi.org/10.1061/(ASCE)0733-9445(2001)127:3(330)).
- Xie, J. and Garber, J. (2014), "HFFB technique and its validation studies", *Wind Struct.*, **18**(4), 375-389. <https://doi.org/10.12989/was.2014.18.4.375>.
- Xu, Y.L., Kwok, K.C.S. and Samaly, B., (1992), "Control of wind-induced tall building vibration by tuned mass damper". *J. Wind Eng. Ind. Aerod.*, **40**(1), 1-32. [https://doi.org/10.1016/0167-6105\(92\)90518-F](https://doi.org/10.1016/0167-6105(92)90518-F).
- Xu, Z. and Xie, J. (2015), "Assessment of across-wind responses for aerodynamic optimization of tall buildings", *Wind Struct.*, **21**(5), 505-521. <https://doi.org/10.12989/was.2015.21.5.505>.